THE JOURNAL OF PHYSICAL CHEMISTRY C

Article

pubs.acs.org/JPCC

In Situ Observation of Dehydration-Induced Phase Transformation from $Na_2Nb_2O_6$–H_2O to $NaNbO_3$

Jong Hoon Jung,*[,†,‡,○] Chih-Yen Chen,[†,§,○] Wen-Wei Wu,[∥,○] Jung-Il Hong,[†,⊥] Byung Kil Yun,[‡] Yusheng Zhou,[†] Nuri Lee,[#] William Jo,[#] Lih-Juann Chen,[§] Li-Jen Chou,[§] and Zhong Lin Wang[†,▽]

[†]School of Materials Science and Engineering, Georgia Institute of Technology, Atlanta, Georgia 30332, United States

[‡]Department of Physics, Inha University, Incheon 402-751, Republic of Korea

[§]Department of Materials Science and Engineering, National Tsing-Hua University, Hsinchu 30313, Taiwan

[∥]Department of Materials Science and Engineering, National Chiao Tung University, Hsinchu 30010, Taiwan

[⊥]Department of Emerging Materials Science, Daegu Gyeongbuk Institute of Science and Technology, Daegu 711-873, Republic of Korea

[#]Department of Physics, Ewha Womans University, Seoul 120-750, Republic of Korea

[▽]Beijing Institute of Nanoenergy and Nanosystems, Chinese Academy of Sciences, Beijing, China

Supporting Information

ABSTRACT: We have monitored the phase transformation from a Sandia octahedral molecular sieve $Na_2Nb_2O_6$–H_2O to a piezoelectric $NaNbO_3$ nanowire through in situ X-ray diffraction (XRD) and transmission electron microscopy (TEM) measurements at high temperatures. After dehydration at 288 °C, the $Na_2Nb_2O_6$–H_2O becomes significantly destabilized and transforms into $NaNbO_3$ with the increase of time. The phase transformation time is exponentially proportional to the inverse of temperature, for example, ~10^5 s at 300 °C and ~10^1 s at 500 °C, and follows an Arrhenius equation with the activation energy of 2.0 eV. Real time TEM investigation directly reveals that the phase transformation occurs through a thermally excited atomic rearrangement due to the small difference of Gibbs free energy between two phases. This work may provide a clue of kinetic control for the development of high piezoelectric lead-free alkaline niobates and a deep insight for the crystallization of oxide nanostructures during a hydrothermal process.

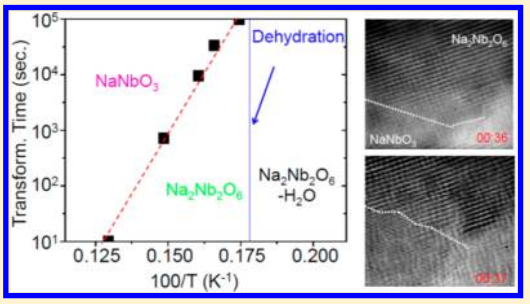

1. INTRODUCTION

As the restriction of hazardous substances is emerging as a major issue, the development of lead-free piezoelectric materials has attracted considerable interest.[1,2] As a strong candidate to replace lead-based piezoelectric materials such as $Pb(Zr,Ti)O_3$, alkaline niobates with perovskite structure such as $(K,Na)NbO_3$ have received great attention due to their high piezoelectricity, high Curie temperature, and electromechanical coupling constant.[3] Until now, however, the reported piezoelectric coefficients of alkaline niobate bulks and thin films are inferior to those of the $Pb(Zr,Ti)O_3$ counterpart, probably due to the volatilization of alkaline ions at high temperature.[4,5] On the other hand, alkaline niobate nanomaterials are free from the volatilization problem due to low temperature synthesis, such as hydrothermal method, through nonequilibrium process.[6] Moreover, the relatively easy control of morphology, size, and shape through nonequilibrium process enables us to investigate the quantum size effects and to widen the applications of alkaline niobate nanomaterials.[7] One of the remaining and challenging issues of alkaline niobate nanomaterials is the increase of piezoelectricity to realize the high performance of lead-free piezoelectric nano devices.

Among alkaline niobate nanomaterials, one-dimensional $NaNbO_3$ nanowires are obtained through the unique crystallization. Under the usual hydrothermal process, $NaNbO_3$ nanocube (rather than nanowire) is crystallized.[8] Prior to the crystallization of $NaNbO_3$ nanocube, it is observed in situ an intermediate crystalline phase, i.e. Sandia octahedral molecular sieve $Na_2Nb_2O_6$–H_2O with nanowire morphology.[9] The $Na_2Nb_2O_6$–H_2O nanowire transforms into $NaNbO_3$ nanowire (not nanocube) after thermal annealing.[10,11] Importantly, the $NaNbO_3$ nanowires are very long, ranging from tens to hundreds of micrometer and have high piezoelectricity.[11] To improve the piezoelectricity of $NaNbO_3$ nanowires for nanogenerator and actuator applications,[12] the in situ investigation on the crystallization should be very important.[9,13−15]

In this paper, we utilized in situ transmission electron microscopy (TEM) in real time at atomic resolution to investigate the phase transformation from $Na_2Nb_2O_6$–H_2O to

Received: August 26, 2012
Revised: October 2, 2012
Published: October 2, 2012

dx.doi.org/10.1021/jp308289r | J. Phys. Chem. C 2012, 116, 22261−22265

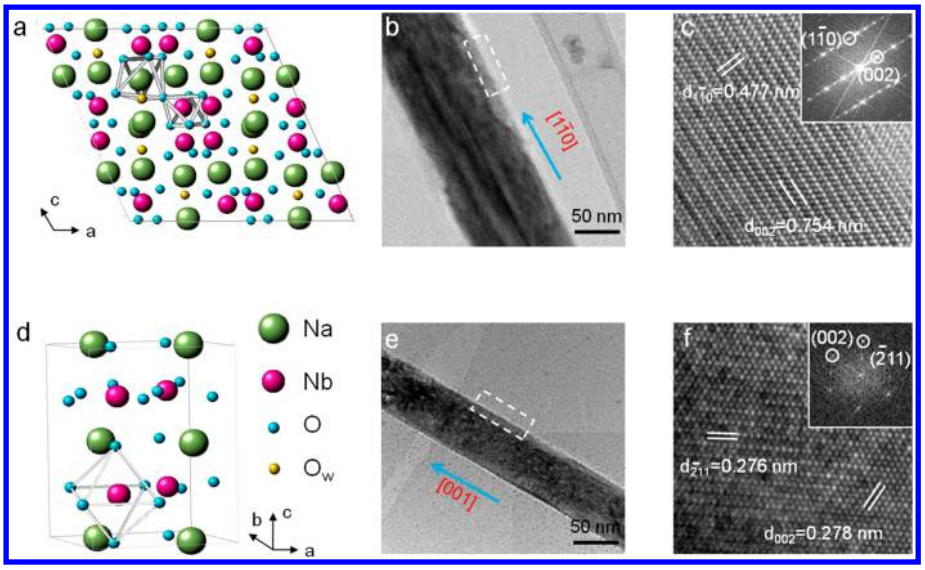

Figure 1. Crystal structure, medium-, and high-resolution transmission electron microscopy (TEM) images of $Na_2Nb_2O_6{-}H_2O$ (a–c) and $NaNbO_3$ (d–f). We show the fast Fourier transform (FFT) patterns for a $Na_2Nb_2O_6{-}H_2O$ along the [110] zone axis (inset of c) and for a $NaNbO_3$ along the [120] zone axis (inset of f). In (a) and (d), we denote Na, Nb, O, and O_w atoms as green, purple, light blue, and orange spheres, respectively. Here, O_w denotes the oxygen atoms in H_2O molecules.

$NaNbO_3$ with the increase of temperature. Combined with in situ X-ray diffraction (XRD), we directly showed that the phase transformation occurs after the dehydration and thermally excited atomic rearrangement is the main mechanism due to small Gibbs free energy difference. This work may provide insight for the growth kinetics during hydrothermal process and possible way for the design of high piezoelectric lead-free alkaline niobate nanowires.

2. EXPERIMENTAL SECTION

The $Na_2Nb_2O_6{-}H_2O$ nanowires were synthesized by the hydrothermal method. In this case, 0.24 mol of NaOH was dissolved in 20 mL of distilled water and then 3.76 mmol of Nb_2O_5 was added into the solution. The thoroughly stirred solution was transferred into a 25 mL Teflon lining in a stainless steel autoclave to undergo a hydrothermal reaction at 150 °C for 4 h. The as-grown $Na_2Nb_2O_6{-}H_2O$ nanowires were further annealed at 300 and 600 °C for 12 h to obtain $Na_2Nb_2O_6$ and $NaNbO_3$ nanowires, respectively. The dehydration and phase transition were examined by thermogravimetry (TG) and a differential scanning calorimetry (DSC) measurements, respectively. For these measurements, the temperature was slowly increased (~10 °C/min). Fourier transform infrared (FT-IR, Bruker VERTEX 80 V) spectroscopy measurement was used to investigate the presence of water. For FT-IR spectroscopy measurement, the nanowires were mixed with KBr powder and dried at 120 °C for 12 h.

High-resolution in situ XRD patterns were obtained via a Panalytical X'Pert Pro diffractometer with Cu Kα radiation. As-grown nanowires were placed in an Anton-Paar HTK 1200 furnace and heated up to 600 °C. To monitor the phase transformation with temperature, the scanning was performed during 30 min after the stabilization of given temperatures. To monitor the phase transformation with time at a given temperature, in addition, the scanning was performed within 1 min repeatedly for the diffraction angles of 2θ = 11–14° and 2θ = 31–34°.

High-resolution in situ TEM measurements were carried out by using a JEOL 2000 V UHV-TEM instrument (base pressure ~3×10^{-10} Torr) with a heating stage up to 1000 °C. During the real time observation, the temperature can be controlled simultaneously and the video recorder has a time resolution of 1/30 s. Fast Fourier transform technique was used to filter the noise of the high-resolution images.

3. RESULTS AND DISCUSSION

In Figure 1, we show the two different crystalline structures of $Na_2Nb_2O_6{-}H_2O$ and $NaNbO_3$. The $Na_2Nb_2O_6{-}H_2O$ consists of NaO_6 and NbO_6 octahedra, as marked by chemical bonding, and the remaining Na ions occupy sites in channels running along [010] (Figure 1a). The NbO_6 octahedra are connected to form double chains along [010], whereas the NaO_6 octahedra are connected into layers parallel to (001). The NaO_6 layers alternate with the layers containing NbO_6 double chains along [001] direction.[16] Peculiarly, the oxygen atoms in H_2O molecules, denoted as yellow spheres (O_w), take part in the chemical bonding with several Na ions to form NaO_6 octahedra. On the other hand, the $NaNbO_3$ consists of NbO_6 octahedra, as marked by chemical bonding, and Na ions (Figure 1d). The NbO_6 octahedra connect to neighboring ones by corner sharing, as expected in the perovskite structure. Importantly, the Nb ions in NbO_6 octahedra are not located at the center but shifted along ⟨001⟩ directions. Hence, an electric polarization is spontaneously formed, which gives rise to the piezoelectricity of $NaNbO_3$.

Medium-, high-resolution transmission electron microscopy (TEM), and fast Fourier transform (FFT) images are shown for $Na_2Nb_2O_6{-}H_2O$ (Figure 1b, c) and $NaNbO_3$ (Figure 1e, f). Both $Na_2Nb_2O_6{-}H_2O$ and $NaNbO_3$ have the nanowire morphology and have high crystalline quality as evidenced by clear lattice fringes. The $Na_2Nb_2O_6{-}H_2O$ nanowire grows along [1–10] and has monoclinic crystal structure (a = 17.114 Å, b = 5.0527 Å, c = 16.5587 Å, and β = 113.947°) with $C2/c$ symmetry. On the other hand, the $NaNbO_3$ nanowire grows

dx.doi.org/10.1021/jp308289r | J. Phys. Chem. C 2012, 116, 22261–22265

along [001] and has orthorhombic crystal structure (a = 5.567 Å, b = 7.764 Å, and c = 5.515 Å) with $P21ma$ symmetry.[17]

As explained in the Experimental Section, the $NaNbO_3$ nanowires are obtained through the thermal annealing of the $Na_2Nb_2O_6$–H_2O. While the morphologies of $Na_2Nb_2O_6$–H_2O and $NaNbO_3$ are nearly the same (Supporting Information, Figure S1), the piezoelectric properties are significantly different. Piezoresponse force microscopy (PFM) amplitude and phase images clearly suggest that the piezoelectricity of $NaNbO_3$ nanowire is strong while that of $Na_2Nb_2O_6$–H_2O is negligible (Supporting Information, Figure S2).

To obtain insight about the phase transformation, we show thermogravimetry (TG) and differential scanning calorimetry (DSC) results in Figure 2a. For these measurements, we

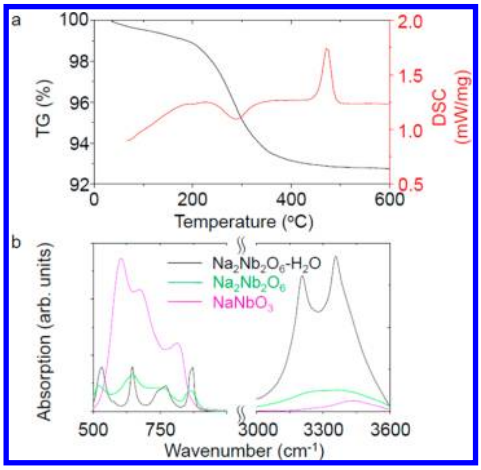

Figure 2. (a) Thermogravimetry (TG) and differential scanning calorimetry (DSC) results of $Na_2Nb_2O_6$–H_2O with the increase of temperature. (b) Fourier transform infrared (FT-IR) absorption spectrum of $Na_2Nb_2O_6$–H_2O (black line), $Na_2Nb_2O_6$ (green line), and $NaNbO_3$ (purple line).

increased temperature slowly (~10 °C/min) to reach thermal equilibrium for each temperature. The mass of $Na_2Nb_2O_6$–H_2O suddenly decreases at ~288 °C, corresponding to an endothermic reaction. After the endothermic reaction, there is one more exothermic reaction at ~474 °C without significant change of mass. From these results, we can infer that the H_2O molecules in $Na_2Nb_2O_6$–H_2O dehydrate at 288 °C and dehydrated $Na_2Nb_2O_6$ transform into $NaNbO_3$ at 474 °C.[16]

In Figure 2b, we show the Fourier transform infrared (FT-IR) absorption spectra of $Na_2Nb_2O_6$–H_2O, dehydrated $Na_2Nb_2O_6$, and $NaNbO_3$ nanowires. The $Na_2Nb_2O_6$–H_2O clearly shows the strong absorption peaks from H_2O molecules near 3200 and 3400 cm^{-1}, while the dehydrated $Na_2Nb_2O_6$ and $NaNbO_3$ show negligible peaks. Optical phonon modes of dehydrated $Na_2Nb_2O_6$ located near 700 cm^{-1} are rather similar to those of $Na_2Nb_2O_6$–H_2O but quite different from those of $NaNbO_3$.

To trace the structural evolution along with the phase transformation, we show the in situ X-ray diffraction (XRD) patterns with the increase of temperature (Figure 3a). The in situ X-ray diffraction patterns clearly show that the crystalline structure changes from $Na_2Nb_2O_6$–H_2O to $NaNbO_3$. For example, the peaks located at $2\theta \sim 10°$ become sharply reduced and broaden, and then finally disappear above 500 °C. On the other hand, the peaks located at $2\theta \sim 32°$ become significantly

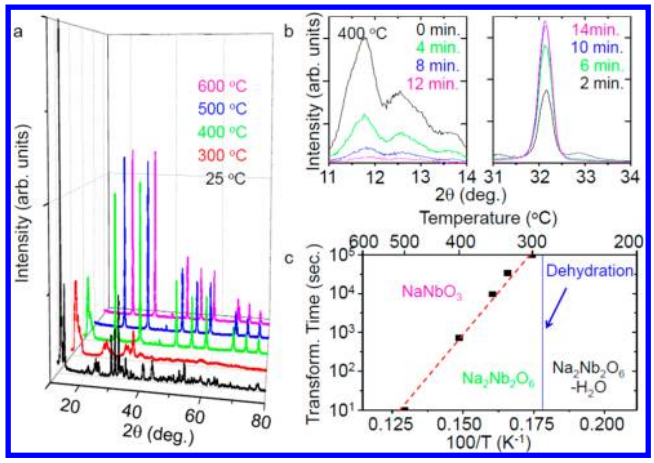

Figure 3. (a) In situ X-ray diffraction (XRD) patterns of $Na_2Nb_2O_6$–H_2O with the increase of temperature. (b) Time evolution of XRD patterns at 400 °C. Left and right panels are shown for the change of representative peaks for $Na_2Nb_2O_6$ and $NaNbO_3$, respectively. (c) Temperature dependence of phase transformation time in log-scale. Below 300 °C, close to dehydration temperature, the phase transformation occurs very slowly (>10^5 s) or not.

reduced at 300 °C and then sharply increase above 400 °C at the different angles.

Interestingly, the dehydrated $Na_2Nb_2O_6$ changes into $NaNbO_3$ with the elapse of time. In Figure 3b, we show the X-ray diffraction patterns at 400 °C at the given elapsed time from the initial measurement. Each diffraction pattern was obtained in 1 min to trace the time evolution of XRD patterns. As representative peaks for $Na_2Nb_2O_6$ and $NaNbO_3$, respectively, we focused the diffraction patterns located at 2θ = 11–14° and 31–34°. The diffraction peaks for $Na_2Nb_2O_6$ (left panel) decrease with time, while those for $NaNbO_3$ (right panel) increase with time. The initial $Na_2Nb_2O_6$ phase is completely transformed into $NaNbO_3$ phase after 12 min. Such a phase transformation does not occur below 300 °C, close to the dehydration temperature, within our measurement time (~800 min). As shown in Supporting Information Figure S3, the phase transformation slowly (quickly) occurs at low (high) temperature.

In Figure 3c, we show the phase diagram for $Na_2Nb_2O_6$–H_2O, $Na_2Nb_2O_6$, and $NaNbO_3$ with temperature and time. Before dehydration, the $Na_2Nb_2O_6$–H_2O does not change at all within our measurement time (~10^5 s). After dehydration, the $Na_2Nb_2O_6$–H_2O changes into $Na_2Nb_2O_6$ and then finally $NaNbO_3$ with the increase of temperature. The destabilized $Na_2Nb_2O_6$, due to the evaporation of oxygen atom (O_w) in NaO_6 octahedra, changes into $NaNbO_3$ as well with the elapse of time. We note that the phase transformation time (t_{ph}) follows a simple Arrhenius equation, that is, $t_{ph} = t_0 \exp(E_g/k_BT)$ with the activation energy of E_g = 2.0 eV.

To investigate the growth kinetics of $NaNbO_3$ from $Na_2Nb_2O_6$ in detail, we conducted in situ TEM measurement in real time at atomic scale. Figure 4 shows a series of in situ high-resolution TEM images obtained at 500 °C. The time shown in each panel represents the elapsed time from the initial measurement. Note that we obtained images at one position for Figure 4a,b and at another position for Figure 4c,d. The interface clearly moves randomly accompanying the phase transformation from $Na_2Nb_2O_6$ to $NaNbO_3$ with the elapse of time. (Real time movement obtained at 500 °C is shown in the Supporting Information, Movie 1.) In consistency with the in

dx.doi.org/10.1021/jp308289r | J. Phys. Chem. C 2012, 116, 22261–22265

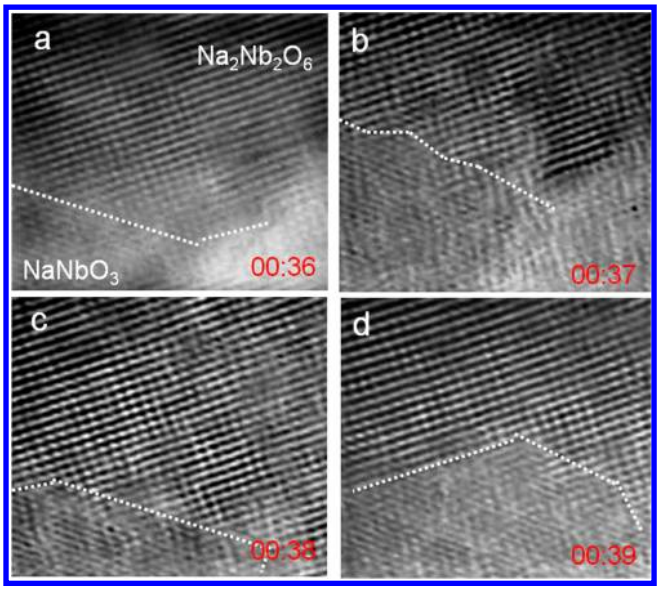

Figure 4. In situ high-resolution TEM image sequences of growing $NaNbO_3$ from dehydrated $Na_2Nb_2O_6$ at 500 °C (from a to d). The white line represents an interface between $Na_2Nb_2O_6$ and $NaNbO_3$. The time shown in each panel is units of minute (first two numbers) and second (second two numbers).

situ XRD results, the phase transformation slowly occurs at 400 °C. (Real time movement obtained at 400 °C is shown in the Supporting Information, Movie 2.)

The detailed in situ TEM movie unambiguously shows that the phase transformation occurs through the atomic rearrangement, rather than oriented attachment after amorphization.[10] Thermally excited atoms will rearrange to their lowest energy sites to form $NaNbO_3$ perovskite structure at the expense of $Na_2Nb_2O_6$. Since the time scale for the crystal growth should be related to the speed of atomic rearrangement, it takes shorter time at higher temperature vice versa.

There are several important points in our in situ XRD and TEM results for the phase transformation from $Na_2Nb_2O_6$–H_2O to $NaNbO_3$. First, it has been known that there are two kinds of phase transformation modes depending on the Gibbs free energy (ΔG) difference between them.[18] If the energy difference is small, fast atomic displacement occurs at an angstrom scale. If the energy difference is large, on the other hand, nucleation for a new crystalline phase and its subsequent growth occurs. In this respect, the observation of atomic displacement rather than nucleation may imply that the ΔG values of dehydrated $Na_2Nb_2O_6$ and $NaNbO_3$ are not so different. Second, many oxide nanostructures are synthesized by the hydrothermal method. Due to the dehydrolysis nature of hydrothermal processes, water is necessary as a solvent and it remains as a product. Therefore, it is necessary to have an insight for the role of water molecules in the crystallization of oxide nanostructures. While we do not directly investigate the phase transformation process from $Na_2Nb_2O_6$–H_2O to $NaNbO_3$ in solution, our observation of dehydration-induced phase transformation might provide an insight into the crystallization of oxide nanostructures during the hydrothermal process.[19,20] Third, there are several important parameters such as water pressure, temperature, reaction time, and precursors which can affect the nucleation of nanomaterials during the hydrothermal reaction. Since the final physical properties of nanomaterials are critically influenced by the kinetic pathway of the phase transformation,[21] our in situ observation may provide a clue for the control of kinetics to develop lead-free alkaline niobates nanowires, including transition metal doped $NaNbO_3$,[22,23] with high piezoelectricity.

4. CONCLUSIONS

We report the direct observation of phase transformation from $Na_2Nb_2O_6$–H_2O to $NaNbO_3$ through in situ X-ray diffraction and transmission electron microscopy measurements. With the increase of temperature, the $Na_2Nb_2O_6$–H_2O transforms into metastable $Na_2Nb_2O_6$ after dehydration and then finally into $NaNbO_3$ without changing the nanowire morphology. Notably, metastable $Na_2Nb_2O_6$ transforms into $NaNbO_3$ with the elapse of time through the atomic rearrangement. Since the $NaNbO_3$ nanowires are quite long and have piezoelectricity without any toxic element such as Pb, our work may provide a clue to realize alkaline niobate nanowires with enhanced piezoelectricity for lead-free piezoelectric nanodevices.

■ ASSOCIATED CONTENT

Ⓢ Supporting Information

Scanning electron miscopy (SEM) images (Figure S1), topology, piezoelectric force microscopy (PFM) amplitude, and phase (Figure S2), in situ X-ray diffraction patterns at 300, 330, 350, and 500 °C (Figure S3), in situ TEM movie at 500 °C (Movie 1), and in situ TEM movie at 400 °C (Movie 2). This material is available free of charge via the Internet at http://pubs.acs.org.

■ AUTHOR INFORMATION

Corresponding Author

*Telephone: +82 (32) 860 7659. Fax: +82 (32) 872 7562. E-mail: jhjung@inha.ac.kr.

Author Contributions

○These authors contributed equally.

Notes

The authors declare no competing financial interest.

■ ACKNOWLEDGMENTS

This work was supported by the Korea Research Foundation Grant funded by the Korean Government (MOEHRD) (KRF-2008-313-C00253).

■ REFERENCES

(1) Cross, L. E. *Nature* **2004**, *432*, 24–25.
(2) Saito, Y.; Takao, H.; Tani, T.; Nonoyama, T.; Takatori, K.; Homma, T.; Nagaya, T.; Nakamura, M. *Nature* **2004**, *432*, 84–87.
(3) Rödel, J.; Jo, W.; Seifert, K. T. P.; Anton, E.-M.; Granzow, T.; Damjanovic, D. *J. Am. Ceram. Soc.* **2009**, *92*, 1153–1177.
(4) Skidmore, A.; Milne, S. J. *J. Mater. Res.* **2007**, *22*, 2265–2272.
(5) Lee, H. J.; Kim, I. W.; Kim, J. S.; Ahn, C. W.; Park, B. H. *Appl. Phys. Lett.* **2009**, *94*, 092902.
(6) Vasco, E.; Magrez, A.; Forró, L.; Setter, N. *J. Phys. Chem. B* **2005**, *109*, 14331–14334.
(7) Hu, Y; Gu, H.; Hu, Z.; Di, W.; Yuan, Y.; You, J.; Cao, W.; Wang, Y.; Chan, H. L. W. *Cryst. Growth Des.* **2008**, *8*, 832–837.
(8) Zhu, H.; Zheng, Z.; Gao, X.; Huang, Y.; Yan, Z.; Zou, J.; Yin, H.; Zou, Q.; Kable, S. H.; Zhao, J.; Xi, Y.; Martens, W. N.; Frost, R. L. *J. Am. Chem. Soc.* **2006**, *128*, 2373–2384.
(9) Modeshia, D. R.; Darton, R. J.; Ashbrook, S. E.; Walton, R. I. *Chem. Commun.* **2009**, 68–70.
(10) Liu, L.; Li, B.; Yu, D.; Cui, Y.; Zhou, X.; Ding, W. *Chem. Commun.* **2010**, *46*, 427–429.

(11) Ke, T.-Y.; Chen, H.-A.; Sheu, H.-S.; Yeh, J.-W.; Lin, H.-N.; Lee, C.-Y.; Chiu, H.-T. *J. Phys. Chem. C* **2008**, *112*, 8827−8831.
(12) Jung, J. H.; Lee, M.; Hong, J.-I.; Ding, Y.; Chen, C.-Y.; Chou, L.-J.; Wang, Z. L. *ACS Nano* **2011**, *5*, 10041−10046.
(13) Pienack, N.; Bensch, W. *Angew. Chem., Int. Ed.* **2011**, *50*, 2014−2034.
(14) Chen, L. J.; Wu, W. W. *Mater. Sci. Eng. R* **2010**, *70*, 303−319.
(15) Strelcov, E.; Davydov, A. V.; Lanke, U.; Watts, C.; Kolmakov, A. *ACS Nano* **2011**, *5*, 3373−3384.
(16) Xu, H.; Nyman, M.; Nenoff, T. M.; Navrotsky, A. *Chem. Mater.* **2004**, *16*, 2034−2040.
(17) Johnston, K. E.; Tang, C. C.; Parker, J. E.; Knight, K. S.; Lightfoot, P.; Ashbrook, S. E. *J. Am. Chem. Soc.* **2010**, *132*, 8732−8746.
(18) Chung, S.-Y.; Kim, Y.-M.; Kim, J.-G.; Kim, Y.-J. *Nat. Phys.* **2009**, *5*, 68−73.
(19) Xu, C.-Y.; Zhen, L.; Yang, R.; Wang, Z. L. *J. Am. Chem. Soc.* **2007**, *129*, 15444−15445.
(20) Rørvik, P. M.; Grande, T.; Einarsrud, M.-A. *Adv. Mater.* **2011**, *23*, 4007−4034.
(21) Burda, C; Chen, X.; Narayanan, R.; El-Sayed, M. A. *Chem. Rev.* **2005**, *105*, 1025−1102.
(22) Nyman, M.; Tripathi, A.; Parise, J. B.; Maxwell, R. S.; Nenoff, T. M. *J. Am. Chem. Soc.* **2002**, *124*, 1704−1713.
(23) Pless, J. D.; Garino, T. J.; Maslar, J. E.; Nenoff, T. M. *Chem. Mater.* **2007**, *19*, 4855−4863.